Electronic Supplementary Material (ESI) for Nanoscale.
This journal is © The Royal Society of Chemistry 2019

Supporting Information

Modulation of oxygen vacancy in tungsten oxide nanosheets for Vis-NIR light-enhanced electrocatalystic hydrogen production and anticancer photothermal therapy

Haiyan Liang, Hongjuan Xi, Shaoqiong Liu, Xuemei Zhang, and Haiqing Liu*

Email: lianghy@sdfmu.edu.cn

This file includes:

S1. Materials

Ammonium tungstate hydrate and hydrochloric acid (HCl) were purchased from Sinopharm Chemical Reagent Co. Ltd. All chemicals were of analytical reagent grade and used without further purification. Solutions were freshly prepared with deionized water.

S2. Characterization Methods

Powder X-ray diffraction (XRD) patterns of the materials were obtained on a diffractometer (Bruker D8) using a Cu Kα radiation source (λ =0.15418 nm) with a 2θ scan from 10° to 90° with a step size of 0.04. X-ray photoelectron spectrometer with a monochromatic Al Kα source (hn ¼ 1486.6 eV) and a charge neutralizer. All the binding energies were calibrated to the C 1s peak at 284.6 eV of the surface adventitious carbon. Scanning electron microscopy (SEM) images were collected using a Hitachi S-4800 microscope equipped with an energy-dispersive X-ray analyser (EDS, Horiba EMAX Energy EX-350). High-resolution TEM (HRTEM) images were obtained using a Philips Tecnai 20U-Twin microscope at an acceleration voltage of 200 kV. The solution of samples was achieved after 10 min ultrasonic pretreatment. The TEM samples were prepared by dropping the primed solution onto a copper grid with polyvinyl formal support film and dried in air. The surface area was determined by Brunauer-Emmett-Teller (BET) measurements with an ASAP 2020 sorptometer. AFM 3100 Digital Instruments Dimension was used to investigate surface morphology. The electron spin resonance (ESR) signals of radical spin-trapped by 2, 2, 6, 6-Tetramethylpiperidinooxy (TEMPO) were examined via a Bruker ER200-SRC spectrometer under visible light irradiation (λ > 420 nm). Raman spectra were obtained using the LabRam HR system from Horiba Jobin Yvon at room temperature with a 532 nm solid laser as the exciting source. UV-*vis* diffuse reflectance spectroscopy spectra (UV-*vis* DRS) was conducted using a Shimadzu UV2550 recording spectrophotometer equipped with an integrating sphere with wavelength of 200 nm to 900 nm. $BaSO_4$ was used as a reference.

S3. Photo/electrochemical Tests

The photoelectrochemical (PEC) test system and electrocatalytic properties of the products for HER were evaluated with a three-electrode system using an electrochemical workstation (CHI 760E). Ag/AgCl (KCl saturated, $E^0_{Ag/AgCl}$ = 0.2046 V, at 25 ^oC) and Pt were used as reference and counter electrodes, respectively. The as-prepared composites were employed as working electrode. The preparation process of the electrode is shown as follows: Firstly, 5 mg sample was dispersed into a mixed solution containing 20 μL 5 wt% Nafion, 800 μL alcohol and 200 μL deionized water. The mixture was under ultrasonic dispersion for 60 min. Then, 100 μL of the homogeneous fresh ink catalyst was directly deposited onto a fluoride-doped thin oxide (FTO) conductive glass plate and then dried at 80 ^oC in a vacuum oven. The loading amount was estimated to be 0.5 $mg \cdot cm^{-2}$ for all samples. A 300 W xenon lamp (PLS-SXE300C, Beijing Perfect Light Company) was used as the light source, providing visible light throughout the photoelectrochemical test. The light intensity was measured with a spectroradiometer (International Light Technologies Model ILT950). Polarization curves of hydrogen generation were obtained using linear sweep voltammetry (LSV) with scan rate of 2 $mV \cdot s^{-1}$ at 25 ^oC in the aqueous solutions (1.0 M KOH) with constant N_2 (g) continually purging for 30 min prior to the measurements. In all measurements, the Ag/AgCl reference electrode was calibrated with respect to the reversible hydrogen electrode (RHE). The potentials of HER measurement were converted to RHE using the equation given by $E_{RHE} = E_{Ag/AgCl} + 0.0591 \times PH + 0.194$, resulting in a shift of +1.0155V versus RHE (1.0 M KOH, pH~13.9). Electrochemical impedance spectroscopy (EIS) was carried out in potentiostatic mode from 10^5 to 0.01 Hz. All the polarization curves are the steady-state ones after several cycles. All polarization curves were IR corrected. The long-term stability test was carried out using chronoamperometry measurements.

S4 Cytotoxicity test

Human Umbilical Vein Endothelial Cells (HUVEC) and MCF-7 cells were first seeded into 96-well cell-culture plates at a density of 1×10^4 cells per well, and then incubated with the sample dispersion at various concentrations (0, 10, 20, 50, 100, and 200 μg·mL-1) in RPMI 1640 medium containing 10% fetal bovine serum (FBS) for 48 h. Afterwards, the cell survival efficiency was measured using CCK-8 assay. The cells cultured with the pure medium were used as a control. The data represented the mean of quintuplicate measurements.

S5 Photothermal ablation of cancer cells

The photothermal effect was evaluated using MCF-7 cells as the test model. MCF-7 cells were seeded on a 24-well plate at a density of 2.5×10^5 cells per well (in RPMI 1640 medium containing 10% FBS, 1.0 mL per well) at 37.0 °C in a humid atmosphere containing 5% CO_2 .After overnight, the sample dispersion (100.0 μg·mL-1) was added for co-incubating for 24h,and then the cells were exposed to NIR laser (808 nm, 2.5 W·cm-^{2}) for 2 min. After laser irradiation, the cells were incubated with fresh RPMI 1640 containing 10% FBS at 37.0 °C for 30 min, and then washed with phosphate buffer saline (PBS) and stained with calcein AM (2.0 μmol·L-1) and PI (3.0 μmol·L-1) for visualization of the live cells and dead cells. Cell viability was evaluated using CCK-8 assay according to the manufacturer suggested procedures. Results were shown as mean ± standard deviation (SD) (n = 4).

S6. Supplementary Figures S1-S12

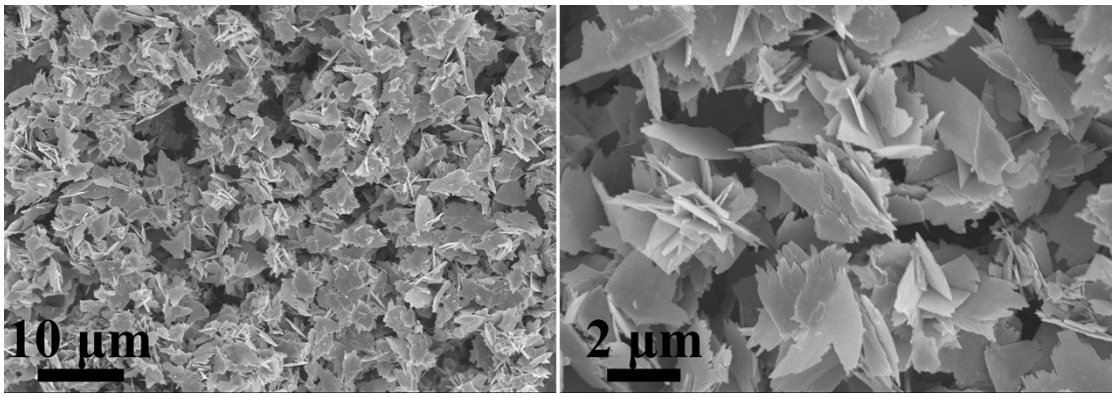

Figure S1. SEM images of precursor HWO_4 nanosheets.

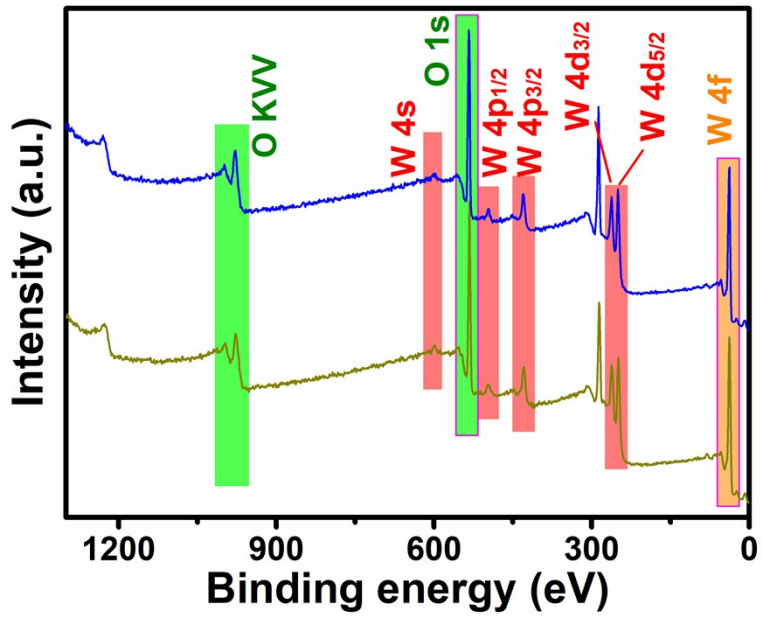

Figure S2. The XPS survey spectrum of precursor HWO_4 and as-synthesized WO_3.

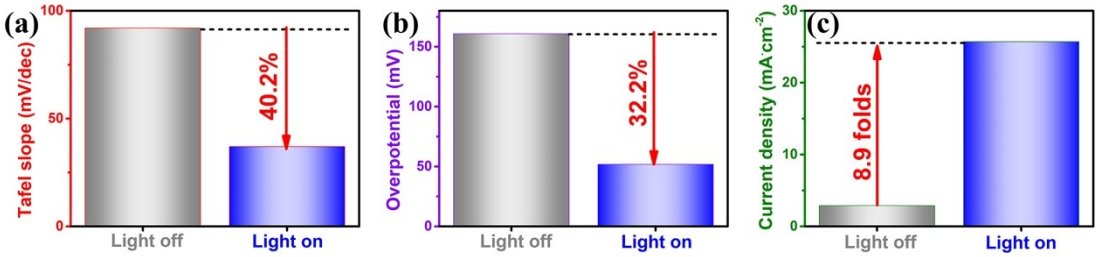

Figure S3. The comparison of tafel slope (a), overpotential (driving 10 $mA \cdot cm^{-2}$) (b) and the current density (at -0.1 V)(c) of as-synthesized WO_3 with and without light irradiation.

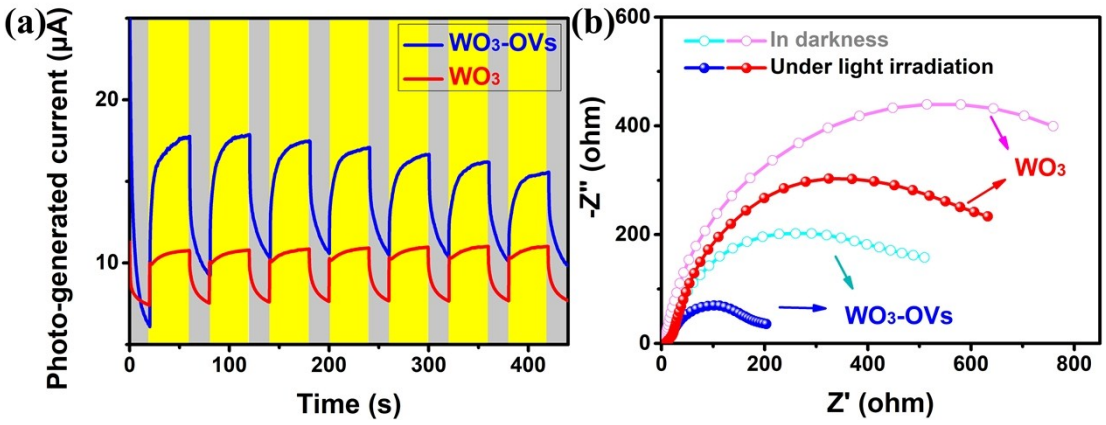

Figure S4. Photo-current responses of WO_3-OVs and WO_3 (a). Influence of light irradiation on Nyquist plots (b).

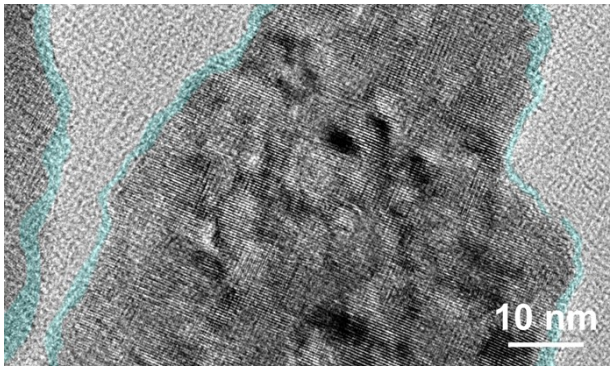

Figure S5. HRTEM image of as-synthesized WO_3-OVs after the PEC stability test.

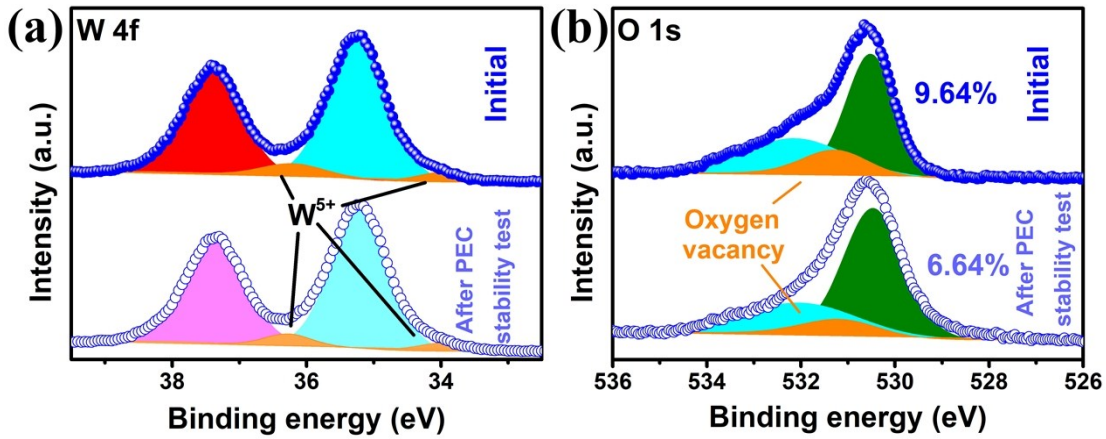

Figure S6. High-resolution XPS spectrum of W 4f region (a) and O 1s region (b) of as-synthesized WO_3 before and after the PEC stability test.

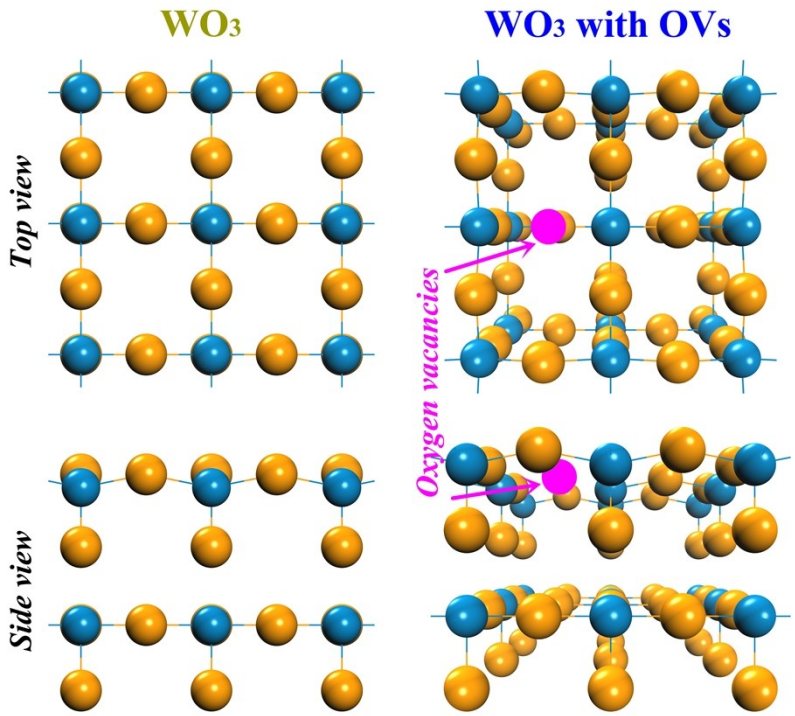

Figure S7. Slab models for WO_3 and WO_3 with OVs.

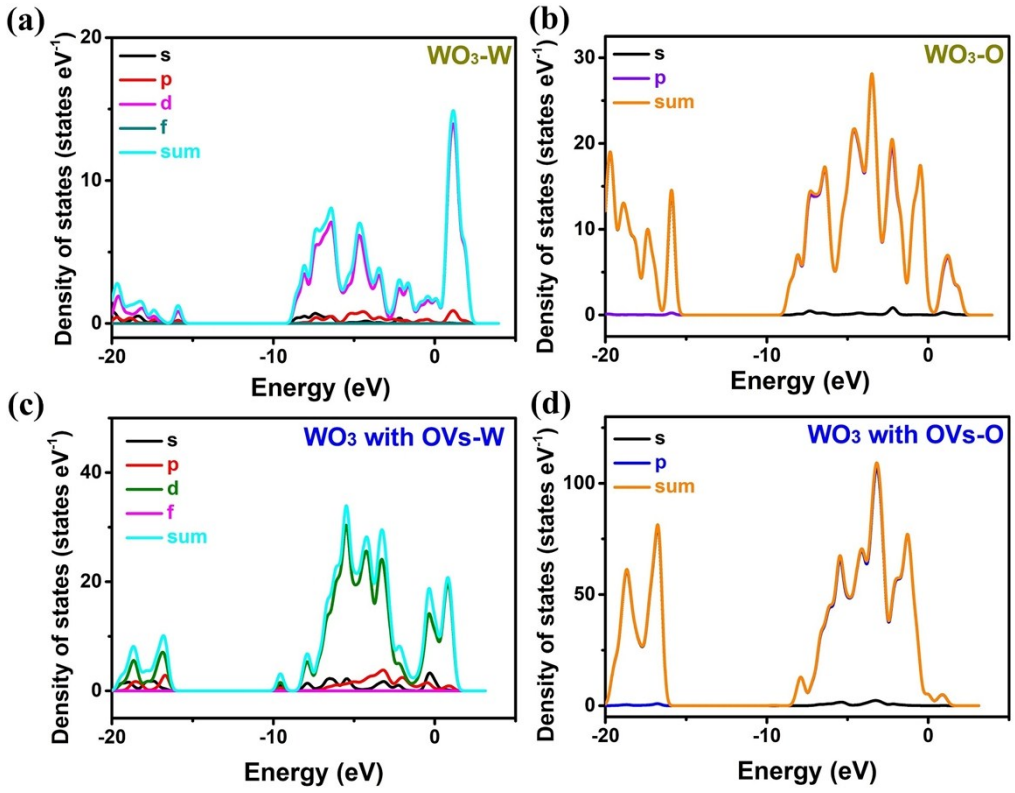

Figure S8. DFT calculated density of states (DOS) of single elements for WO_3 and WO_3 with OVs.

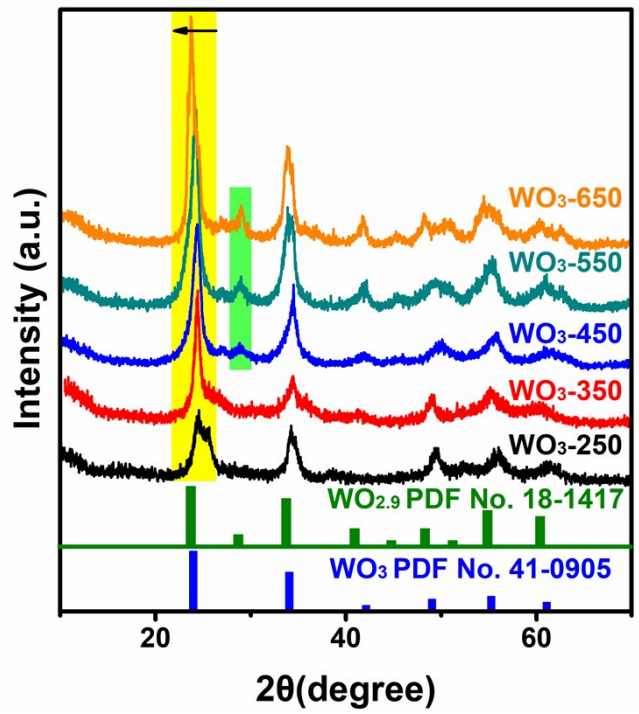

Figure S9. XRD patterns of WO_3 nanosheets with different amount of oxygen vacancies.

As shown in Figure S9, the characteristic (100) peaks of all the samples obviously shifted to the left, which is due to the increase of oxygen vacancy. For WO_3-450/550/650 samples, an additional peak at 28.7° appeared and the corresponding intensity enhanced with calcination temperature. By comparing the standard peaks and combining the synthesis mechanism, we can conclude that this additional peak at 28.7° is the (101) peak of $WO_{2.9}$ (JCPDS No. 18-1417). This result also supports the successful formation and regulation of oxygen vacancy.

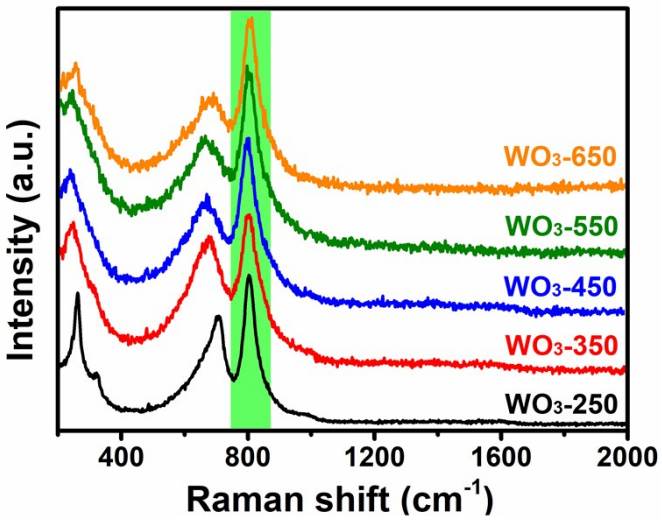

Figure S10. Raman spectrum of WO_3 nanosheets with different amount of oxygen vacancies.

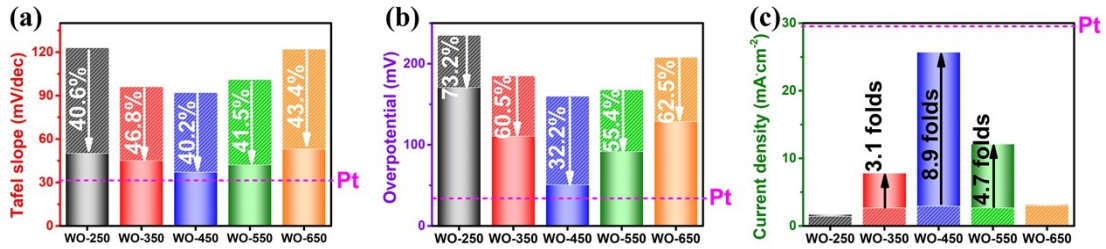

Figure S11. The comparison of tafel slope (a), overpotential (driving 10 $mA \cdot cm^{-2}$) (b) and the current density (at -0.1 V) (c) of WO_3 nanosheets with different amount of oxygen vacancies with and without (shaded column) light irradiation.

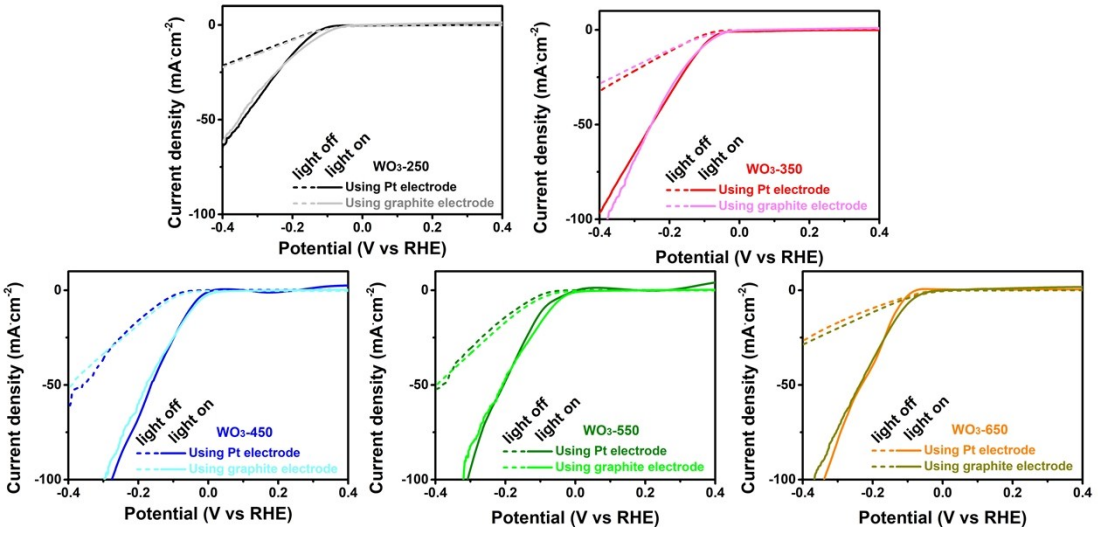

Figure S12. The polarization curves using different counter electrodes at WO_3-

250/350/450/550/650, respectively.

In order to study whether the dissolution and redeposition of Pt sheet occurred during the electrocatalytic HER in our experimental conditions. Graphite and Pt were used to test the influence of counter electrode on electrocatalytic HER, respectively. There is no significant difference about the HER ability between Pt electrode system and graphite electrode system, which avoids the influence of Pt redeposition (Figure S12).

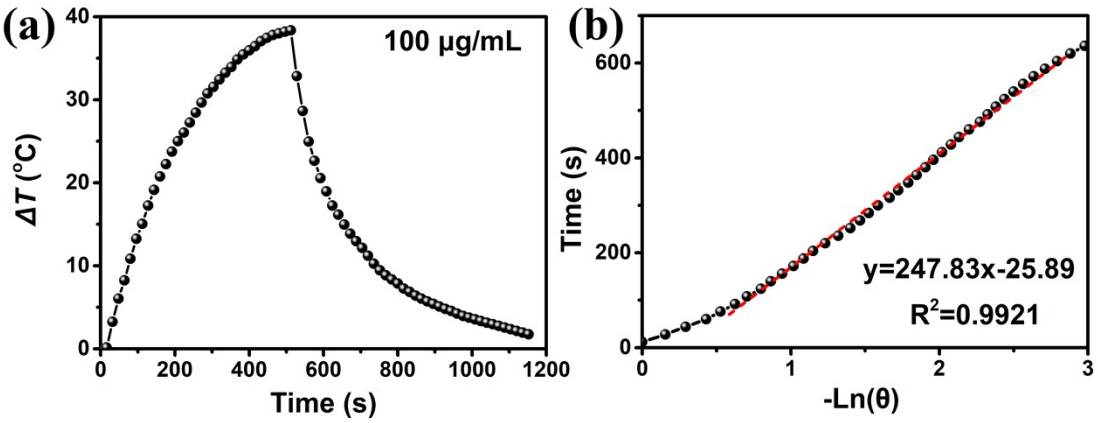

Figure S13. (a) Plot of temperature variation versus the irradiation (2 W/cm^2) duration where the decay section was recorded after the laser was switch off; (b) Linear time data versus-ln (θ) obtained from the cooling period of NIR laser off.

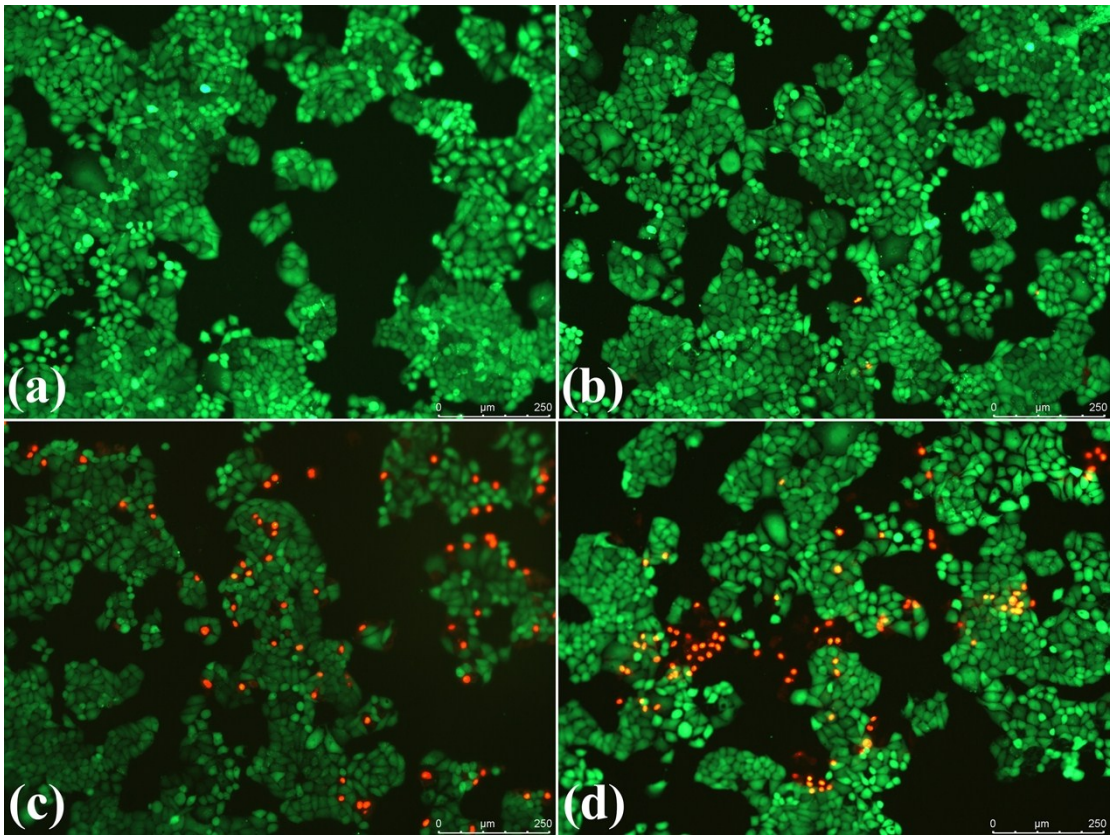

Figure S14. Photothermal destruction of MCF-7 cells treated with laser only and combination of the WO_3-OVs with laser irradiation for 2 min. (a, c) 1.5 $W \cdot cm^{-2}$; (b, d) 2.0 $W \cdot cm^{-2}$.